1521-009X/48/7/553–562$35.00
DRUG METABOLISM AND DISPOSITION

https://doi.org/10.1124/dmd.120.090563
Drug Metab Dispos 48:553–562, July 2020

Concentration Dependence of the Unbound Partition Coefficient Kp_{uu} and Its Application to Correct for Exposure-Related Discrepancies between Biochemical and Cellular Potency of KAT6A Inhibitors[S]

Cornelius Trünkle, Christian Lechner, Daniel Korr, Léa Bouché, Naomi Barak, Amaury Fernández-Montalván, Roderich D Süssmuth, and Andreas Reichel

Bayer AG, Pharma R&D, Translational Sciences, Research Pharmacokinetics, Berlin, Germany (C.T., C.L., A.R.); Bayer AG, Pharma R&D, Therapeutic Compound Research, Berlin, Germany (D.K.); Bayer AG, Pharma R&D, Small Molecule Innovation, Berlin, Germany (L.B., N.B., A.F.-M) and Technische Universität Berlin, Institut für Chemie, Berlin, Germany (C.T., R.D.S.)

Received January 31, 2020; accepted April 7, 2020

ABSTRACT

The unbound partition coefficient (Kp_{uu}) allows the estimation of intracellular target exposure from free extracellular drug concentrations. Although the active mechanisms controlling Kp_{uu} are saturable, Kp_{uu} is commonly determined at a single concentration, which may not be appropriate in cases in which drug concentrations can largely vary, e.g., in plasma in vivo or in vitro IC_{50} assays. We examined the concentration dependence of Kp_{uu} in vitro using KAT6A inhibitors with varying potency drop-off in ZR75-1 breast cancer cells to account for exposure-related discrepancies between cellular and biochemical IC_{50}. Considering saturability resulted in a better quantitative bridge between both IC_{50} values and gave way to a simplified method to determine Kp_{uu} that is suitable for the prediction of unbound cytosolic drug concentrations without the need to generate $f_{u,cell}$ estimates from binding studies in cell homogenates. As opposed to the binding method, which destroys cellular integrity, this approach provides an alternative $f_{u,cell}$ estimate and directly reflects the fraction of unbound drug in the cell cytosol based on Kp saturation ($f_{u,cyto}$) of intact cells. In contrast to the binding method, prediction of intracellular KAT6A exposure with this more physiologic approach was able to bridge the average exposure gap between biochemical and cellular IC_{50} values from 73-fold down to only 5.4-fold. The concept of concentration-dependent Kp_{uu} provides a solid rationale for early drug discovery to discriminate between pharmacology and target exposure–related IC_{50} discrepancies. The attractiveness of the approach also lies in the use of the same assay format for cellular IC_{50}, $f_{u,cyto}$, and the unbound partition coefficient based on $f_{u,cyto}$ ($Kp_{uu,cyto}$) determination.

SIGNIFICANCE STATEMENT

Examination of the yet-unexplored concentration dependence of the unbound partition coefficient led to a new experimental approach that resulted in more reliable predictions of intracellular target exposure and is well suited for routine drug discovery projects.

Introduction

The unbound partition coefficient (Kp_{uu}) is emerging as a powerful parameter to estimate the unbound drug exposure of intracellular targets (Guo et al., 2018). Whereas the drug exposure of extracellular targets can be directly approximated from unbound plasma concentrations for most tissues, the estimation of unbound intracellular concentrations requires knowledge of the processes that control intracellular drug disposition. Kp_{uu} thus corresponds to the ratio of the free drug concentrations inside and outside of the cell, which are a net result of complex cellular mechanisms such as passive membrane diffusion, transporter-mediated uptake and/or efflux, cellular metabolism, nonspecific binding, and sequestration to organelles (Zheng et al., 2011; Li et al., 2018). Kp_{uu} quantitatively describes the extent of an unbound drug concentration asymmetry between the intracellular and extracellular space at steady state. Kp_{uu} values around unity are indicative of predominantly passive drug distribution processes, whereas Kp_{uu} values >1 suggest active drug uptake into cells, and Kp_{uu} values <1 are indicative of drug efflux out of the cell (Zhang et al., 2019).

Currently, there are various methods available to estimate Kp_{uu} experimentally. They all have in common the consideration of Kp_{uu} as a single value (Riede et al., 2017; Yoshikado et al., 2017). This seems counterintuitive given the principal saturability of underlying mechanisms such as drug uptake, efflux, metabolism, and lysosomal trapping (Sugano et al., 2010; Schmitt et al., 2019). We therefore set out to

This work was financed by Bayer AG, Germany.
Primary laboratory of origin: (Bayer AG, Berlin, Germany).
https://doi.org/10.1124/dmd.120.090563.
[S]This article has supplemental material available at dmd.aspetjournals.org.

ABBREVIATIONS: $f_{u,cell}$, fraction of unbound drug in the cell; $f_{u,cell,hom}$, fraction of unbound drug in the cell based on binding in cell homogenate; $f_{u,cyto}$, fraction of unbound drug in the cell cytosol based on Kp saturation; $IC_{50,biochem}$, biochemical potency; $IC_{50,cell}$, cellular potency; KAT6A/MYST3 K-Acetyltransferase 6AKp, partition coefficient; Kp_{uu}, unbound partition coefficient; $Kp_{uu,cell,hom}$, unbound partition coefficient based on $f_{u,cell,hom}$; $Kp_{uu,cyto}$, unbound partition coefficient based on $f_{u,cyto}$; LC-MS/MS, liquid chromatography-tandem mass spectrometry; TR-FRET, time-resolved fluorescence energy transfer.

examine 1) the concentration dependence of Kp_{uu} in vitro and 2) its impact on unbound intracellular target exposure. We hypothesized that Kp_{uu} does not assume a constant value but is rather changing with the extent of saturation. This implicates that the unbound drug concentration asymmetry between the cytosolic and extracellular space is maximal at low extracellular compound concentrations and will become less pronounced with increasing concentrations until passive permeation prevails. The unbound drug concentrations on both sides of the plasma membrane will then converge, and Kp_{uu} approaches 1 (see Fig. 1). The concentration dependence of Kp_{uu} may be of particular interest when trying to elucidate whether potential discrepancies between biochemical and cellular IC_{50} values, the so-called cellular potency drop-off (Hann and Simpson, 2014), may be due to either 1) differences in the intracellular target exposure or 2) the target responding differently in the high complexity of a living cell.

In addition, drug sequestration from the cytosol to subcellular compartments like lysosomes and mitochondria due to pH gradients and differences in membrane potential can significantly affect cytosolic unbound drug concentrations (Rajendran et al., 2010; Li et al., 2018; Schmitt et al., 2019). Previously published methods for the determination of Kp_{uu} assume an average unbound drug concentration of all cellular compartments. In this study, we propose a novel approach to estimate the amount of unbound drug available specifically in the cytosolic compartment ($Kp_{uu,cyto}$) that is based on saturation of active mechanisms involved in cellular drug disposition.

To test our hypothesis, we have investigated a set of structurally related inhibitors of histone acetyltransferase KAT6A, also known as MYST3, that induce senescence via the INK4A-ARF pathway (Sheikh et al., 2015) and have recently been identified as frequently overexpressed oncogenic targets in breast cancers like mammalian ductal carcinoma ZR75-1 (Yu et al., 2017). Compounds were selected from literature (Baell et al., 2018) and an in-house program based on their potency against ZR75-1 cells compared with isolated recombinant KAT6A in biochemical potency measurements. KAT6A is located in the cell nucleus, which is directly connected to the cytosol through nuclear pore complexes that are large enough to allow rapid and free diffusion of molecules up to 5000 Da (Naim et al., 2007; Alberts, 2008; Timney et al., 2016). In a cellular system, target exposure of KAT6A is therefore assumed to be equal to the unbound drug concentration in the cytosol.

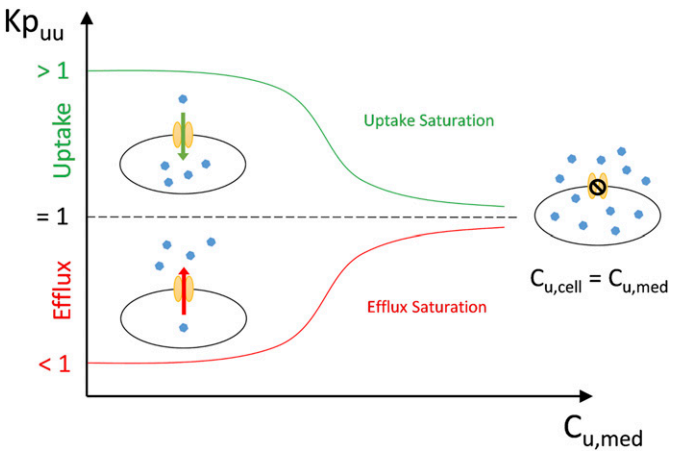

Fig. 1. Hypothesis for the concentration dependence of Kpuu in the presence of active cellular uptake and efflux mechanisms. The unbound drug concentration asymmetry between the intracellular ($c_{u,cell}$) and extracellular ($c_{u,med}$) space is maximal at low concentrations and becomes less pronounced with increasing drug concentrations in the extracellular space as active transport across the plasma membrane is being saturated. In the fully saturated state, unbound drug concentrations on both sides of the plasma membrane will be equal, and $Kp_{uu} = 1$.

With ZR75-1 cells expressing tumor drug resistance–associated efflux transporters such as ABCB1 (multidrug resistance protein 1) and ABCC1 (multidrug resistance–associated protein 1) (Faneyte et al., 2001; Lemos et al., 2009; Oba et al., 2016), the concept of the concentration-dependent Kp_{uu} will be applied to 1) improve our understanding of the relationship between intracellular and extracellular unbound drug concentrations, 2) overcome the limitations of the frequently used in vitro cell homogenization method (Mateus et al., 2013), and 3) derive a rationale for early drug discovery to more clearly discriminate between pharmacology or target exposure–related discrepancies between biochemical and cellular potency assays.

Materials and Methods

Materials and Compounds. Reagents for cell culture and experiments were obtained from Thermo Fisher Scientific (Waltham, MA) or Sigma-Aldrich (St. Louis, MO). The adherent mammary gland ZR75-1 breast carcinoma cell line used in this study originated from ATCC® (catalog number CRL-1500). Inhibitors of KAT6A were synthesized at Bayer AG laboratories or provided from an in-house compound screening library with purities >95%. DMSO stock solutions at a final concentration of 10 mM were prepared for all compounds and stored at −80°C for further use. Physicochemical compound properties ($logD_{pH7.5}$, pK_a, and charge state) were predicted in silico using ADMET Predictor (Simulations Plus Inc.). Predictions of logD values were based on an in-house software algorithm that was trained with experimental HPLC retention time data of 76.548 reference compounds, as recently described by Montanari et al. (2019). Caco-2 permeability was determined during routine preclinical in vitro compound characterization as previously described (Nguyen et al., 2019).

Cell Culture. ZR75-1 cells were cultivated at 37°C in a 95% relative humidity and 5% CO_2 atmosphere in gibco RPMI 1640 medium containing GlutaMAX and 10% FCS (Life Technologies, Carlsbad, CA). Cells were passaged weekly after reaching ~80% confluency according to the ATCC® manufacturing protocol. Cellular volume was microscopically determined from the diameter, d, of suspended cells, assuming spherical cell shape (d = 15.9 ± 2.5 µm; n = 500). In all, 10^6 cells were lysed in RIPA lysis buffer (pH 7.5; Tris-HCl 50 mM, NaCl 150 mM, EDTA 2 mM, and 1% Triton X-100) for the normalization of cellular volume to protein content (V = 9.5 ± 1.3 µl/mg; n = 3) using Pierce BCA protein assay kit (Pierce Biotechnology, Rockford, IL).

Biochemical KAT6A Potency Screen. KAT6A inhibitory activity of the compounds was quantified using the time-resolved fluorescence energy transfer (TR-FRET) assay, which measures acetylation of a histone H4-derived peptide with amino acid sequence SGRGKGGKGLGKGGAKRHRKVLRDK-biotin (Biosyntan GmbH, Berlin, GER) by recombinant human His-tagged KAT6A protein (amino acids 194–810), purified in-house from baculovirus-infected insect cells (Sf9) similarly as previously described by Dreveny et al. (2014). Assay mixtures containing KAT6A (0.6 nM), H4 peptide (220 nM), CoASAc (600 nM), and test compounds (0.01–20 µM in 11-point, 3.5-fold serial dilutions) in assay buffer (25 mM Tris-HCl, pH 8.0, 25 mM NaCl, 1 mM EGTA, 2.5 mM glutathion, 0.02% w/v chicken albumin, 0.05% Pluronic F127) were incubated for 60 minutes at room temperature in black 384-well low-volume microtiter plates (Greiner Bio-One GmbH, Frickenhausen, Germany). In a subset of low- and high-activity control wells, KAT6A and test compounds were replaced either by assay buffer or by vehicle (1% DMSO). The enzymatic reaction was stopped and its products were detected by addition of 100 µM anacardic acid (Enzo Life Sciences Inc., Farmingdale, NY), 1 nM anti-histone H4 (acetyl K8) antibody (abcam, Cambridge, UK), 0.5 nM anti-rabbit IgG Eu (PerkinElmer, Waltham, MA), and 22 nM SAXL-665 (Cisbio, Codelet, France) in 25 mM HEPES, pH 7.5, 0.1% bovine serum albumin. TR-FRET signals were acquired in a RUBYstar or PHERAstar microplate reader (both BMG Laboratory Technologies, Offenburg, Germany) to quantify the amount of acetylated peptide by the ratio of fluorescence emissions at 620 nm and 665 nm upon excitation at 337 nm. Biochemical IC_{50} values were calculated by fitting the normalized TR-FRET data to a four-parameter logistic equation using Genedata Screener software (Genedata AG, Basel, Switzerland).

Cellular ZR75-1 Potency Screen. ZR75-1 cells were suspended in cell culturing medium and plated at a final density of 3000 cells per well in a 96-well microtiter plate on the day prior to the experiment. Plates were incubated at 37°C in a 95% relative humidity and 5% CO_2 atmosphere overnight for cell attachment.

On the day of the experiment, the culturing medium was replaced by incubation medium (RPMI 1640 medium containing GlutaMAX and 2.5% FCS). Compounds were added from 10 mM DMSO stock solution to the desired concentrations (0.002–40 μM; triplicate measurements) and incubated over 6 days. Cell viability was determined by staining cells with Alamar Blue Reagent (Invitrogen, Carlsbad, CA) for 2 hours, followed by fluorescence measurements in a Victor ×3 MTP-Reader (excitation at 530 nm; emission at 590 nm; PerkinElmer). Measurements were normalized for DMSO-only treated cells, and cellular IC_{50} values were determined by curve fitting in analogy to the biochemical potency assay. Based on these data, the occurrence of cytotoxic effects at high test compound concentrations that could potentially impact Kp measurements in ZR75-1 cells was evaluated. As cytotoxic effects would have resulted in negative percentage values of cell growth relative to untreated control cells, which was not observed for any of the compounds used in this study (Supplemental Fig. 3), cytotoxicity is not expected to affect the accuracy of the Kp measurements in this study.

Measurements of Concentration-Dependent Kp. ZR75-1 cells were suspended in cell culture medium and seeded in Corning tissue-culture–treated 48-well plates (Corning Inc., Corning, NY) at a density of 100,000 cells per well on the day prior to the experiment. Plates were incubated at 37°C in a 95% relative humidity and 5% CO_2 atmosphere overnight for cell attachment. Compound solutions with final concentrations ranging from 0.1 to 100 μM were prepared in the same incubation medium that was used in the cellular potency screen, with the final DMSO concentration not exceeding 1% at the highest concentration tested, which is not expected to interfere with the overall assay readout. Cells were washed twice with incubation medium before applying 200 μl of compound solution (t_0) and incubating at 37°C for 45 minutes on a heated orbital plate shaker at low speed. For each compound and concentration, triplicate incubations were conducted. After the incubation, the overlaying medium (t_{45}) was harvested and cells were washed twice with ice-cold gibco PBS, pH 7.4 (Life Technologies) and lysed for 5 minutes under fast shaking by adding 200 μl methanol containing 0.1 μM of an internal LC-MS standard. Cell lysates (for c_{cell}) and medium samples (for c_{med}) at t_0 and t_{45} were transferred to a 96-well analytical plate, diluted with methanol/0.1 μM internal standard, and stored overnight at −80°C. Prior to sample quantification via LC-MS/MS, the analytical plate was centrifuged for 15 minutes at 3700 rpm at 4°C for protein precipitation. Cellular volume (V_{cell}) was determined in representative wells by washing cells twice with ice-cold PBS followed by lysis with RIPA lysis buffer (pH 7.5) and protein quantification (Pierce BCA protein assay kit). The total cellular Kp in ZR75-1 cells was calculated according to

$$Kp = \frac{c_{cell}}{c_{med}} = \frac{\left(\frac{A_{cell}}{V_{cell}}\right)}{c_{med}} \quad (1)$$

Total compound recovery from cell and medium after the incubation was calculated according to

$$Recovery[\%] = \frac{A_{cell} + A_{med,t45}}{A_{med,t0}} * 100 \quad (2)$$

with A_{cell} being the amount of compound in the cell lysate, $A_{med,t45}$ the amount of compound in the medium at the end of the incubation, and $A_{med,t0}$ the amount of compound in the medium prior to the incubation.

To mathematically describe the concentration dependence of total cellular drug accumulation, curve fitting of the following equation to Kp measurements (0.1–100 μM) was performed for each compound using SigmaPlot 13 (Systat Software GmbH):

$$Kp = Kp_{unsat} + \frac{Kp_{sat} - Kp_{unsat}}{1 + \left(\frac{c_{med}}{K_{m,app}}\right)^{-Hillslope}} \quad (3)$$

where Kp_{unsat} represents the total cellular accumulation in the presence of unsaturated active mechanisms, and Kp_{sat} represents the total cellular accumulation at the fully saturated state. $K_{m,app}$ describes the total extracellular concentration at which saturation is half-maximal. The percentage of full saturation that is achieved at the highest applied concentration in the medium (100 μM) was calculated according to

$$Saturation[\%] = \frac{Kp_{100\mu M}}{Kp_{sat}} * 100 \quad (4)$$

Determination of $f_{u,med}$. Binding of the test compounds to the extracellular incubation medium (RPMI 1640 with GlutaMAX and 2.5% FCS) was determined via rapid equilibrium dialysis. The HTD96b equilibrium dialysis chamber (HTDialysis LLC, Gales Ferry, CT) was assembled according to the manufacturing protocol. The dialysis membranes with a molecular mass cutoff of 12–14 kDa (HTDialysis LLC) were prepared 1 day prior to the experiment and stored at 4°C in 50 mM dialysis phosphate buffer (40.5 mM $Na_3HPO_4{\cdot}3H_2O$, 9.5 mM $Na_3H_3PO_4{\cdot}H_2O$, 9 g/l NaCl, pH 7.4) by bathing them in double distilled H_2O for 30 minutes, followed by 15 minutes in 30% ethanol and three washing steps in double distilled H_2O. Compound solutions with a final concentration of 1 μM were prepared from 10 mM DMSO stock solutions in incubation medium. One hundred fifty microliters of compound solution (t_0) was added to the donor compartment of the dialysis device and dialyzed against 150 μl of 50 mM dialysis phosphate buffer in the receiver compartment for 7 hours at 37°C under low orbital shaking. Dialysis was performed in quadruplets for each compound. Additionally, triplicates of 1 μM control compound buffer solutions were dialyzed against buffer to determine whether steady-state conditions are achieved between the donor and receiver compartment. After the incubation, samples from the donor and receiver compartment (t_{7h}) as well as compound solution (t_0) for the determination of recovery were transferred to a 96-well analytical plate. Incubation medium and 50 mM dialysis phosphate buffer were added to yield identical sample matrices and further diluted with 400 μl methanol containing 0.1 μM internal standard. Samples were stored overnight at −80°C and centrifuged at 3700 rpm and 4°C for protein precipitation prior to LC-MS/MS analysis. Compound recovery was determined to be >90%, whereas equilibrium between donor and receiver compartments was achieved to >95% (data not shown). Binding to the extracellular incubation medium was calculated according to

$$f_{u,med} = \frac{c_{Receiver}}{c_{Donor}} \quad (5)$$

Theoretical Considerations Regarding the Concentration Dependence of Kp_{uu}. Generally, the cellular unbound partition coefficient Kp_{uu} is described by the following equation:

$$Kp_{uu} = \frac{c_{u,cell}}{c_{u,med}} = Kp * \frac{f_{u,cell}}{f_{u,med}} \quad (6)$$

Alternatively, Kp_{uu} can be described mechanistically by the kinetics of all mechanisms that are involved in cellular drug disposition and thereby determine the intracellular unbound drug concentration at steady state (extended clearance model Varma et al. (2015)):

$$Kp_{uu} = \frac{CL_{diff} + CL_{in,act}}{CL_{diff} + CL_{ef,act} + CL_{met}} \quad (7)$$

where CL_{diff} is the rate of passive diffusion across the plasma membrane, $CL_{in,act}$ is the transporter-mediated uptake clearance, $CL_{ef,act}$ is the transporter-mediated efflux clearance from the cell, and CL_{met} is the rate by which the compound is cleared through cellular metabolism. As all active processes are characterized by substrate concentration-dependent saturability, concentrations on both sides of the cytosolic membrane will be equal in the fully saturated state (Kp_{sat}), and Kp_{uu} will approach 1 with increasing drug concentrations:

$$Kp_{uu} = \frac{CL_{diff}}{CL_{diff}} = Kp_{sat} * \frac{f_{u,cell}}{f_{u,med}} = 1 \quad (8)$$

We therefore introduced a novel method for the determination of Kp_{uu} that is based on the saturability of the underlying mechanisms, called $Kp_{uu,cyto}$ subsequently, and compared it to the commonly used parameter $Kp_{uu,cell,hom}$, determined with the binding method.

Determination of $f_{u,cyto}$ and $Kp_{uu,cyto}$ Using the Novel Saturation Method. As Kp_{sat} is representative of total cellular accumulation, including binding and subcellular sequestration, the fraction of unbound drug available only

in the cytosolic compartment of the cell can be derived from Kp_{sat} by rearranging eq. 8 to

$$f_{u,cyto} = \frac{1}{Kp_{sat}} * f_{u,med} \quad (9)$$

Based on the common assumption that $f_{u,cell}$—and, hence, also $f_{u,cyto}$—is not concentration-dependent (Mateus et al., 2013) the unbound partition coefficient $Kp_{uu,cyto}$ at various extracellular concentrations was calculated according to

$$Kp_{uu,cyto} = Kp * \frac{f_{u,cyto}}{f_{u,med}} = Kp * \frac{1}{Kp_{sat}} \quad (10)$$

Simplified Approach to Determine $Kp_{uu,cyto}$. In this study, we were able to discriminate between an unsaturated (Kp_{unsat}) and fully saturated state (Kp_{sat}) in total cellular accumulation. Consequently, it is not necessary to measure Kp over a large concentration range to estimate $Kp_{uu,cyto}$, as only two Kp measurements, one determined at a low, nonsaturating (i.e., 0.1 μM) concentration and the other at a high, saturating concentration (i.e., 100 μM), can provide good estimates of both states:

$$Kp_{uu,cyto} = Kp_{0.1\mu M} * \frac{1}{Kp_{100\mu M}} \quad (11)$$

Determination of $f_{u,cell,hom}$ and $Kp_{uu,cell,hom}$ Using the Binding Method (Mateus et al., 2013). To obtain tissue homogenates, suspended ZR75-1 cells were counted, washed twice with warm PBS, centrifuged at 160*g* for 5 minutes, and resuspended to a final cell concentration of 10^6 cells/ml in 50 mM dialysis phosphate buffer (40.5 mM $Na_3HPO_4 \cdot 3H_2O$, 9.5 mM $Na_3H_3PO_4 \cdot H_2O$, 9 g/l NaCl, pH 7.4). The suspension was homogenized with a B. Braun POTTER S Homogenizer (Sartorius AG, Göttingen, Germany) at 700 rpm and 20 strokes. Protein content of the homogenate was determined with Pierce BCA protein assay kit to calculate cellular volume and the dilution factor D of the homogenate (ranging from 29 to 42). ZR75-1 homogenates were stored at –80°C for a maximum of 3 days before binding measurements were conducted with rapid equilibrium dialysis. The experimental procedure was in analogy to the determination of $f_{u,med}$, using cell homogenate instead of incubation medium. Although steady-state conditions between the donor and receiver compartment were achieved (>95%), total compound recovery from the dialysis chamber at t_{7h} ranged from 21% to 100%, with lower recovery observed for highly bound compounds (data not shown). The following equation was used to determine compound binding to tissue homogenate:

$$f_{u,hom} = \frac{c_{Receiver}}{c_{Donor}} \quad (12)$$

Cellular binding was subsequently scaled from $f_{u,hom}$ with the dilution factor D to account for homogenate dilution according to

$$f_{u,cell,hom} = \frac{1}{D * \left(\frac{1}{f_{u,hom}} - 1\right) + 1} \quad (13)$$

The unbound partition coefficient $Kp_{uu,cell,hom}$ was calculated according to

$$Kp_{uu,cell,hom} = Kp_{unsat} * \frac{f_{u,cell,hom}}{f_{u,med}} \quad (14)$$

Kp_{unsat} was used for the calculation of $Kp_{uu,cell,hom}$, as Kp is generally determined at low extracellular concentrations and, therefore, most likely represents the unsaturated state.

Prediction of Intracellular KAT6A Target Exposure. Kp_{uu} obtained with the two methods was parallelly applied for the prediction of KAT6A exposure in ZR75-1 cells and the corresponding potency value. The predicted values were then compared with measurements of biochemical potency ($IC_{50,biochem}$) against isolated KAT6A in vitro.

1. Using Kp_{uu} from the binding method (i.e., $Kp_{uu,cell,hom}$) to predict the intracellular IC_{50}, without consideration of saturation effects according to:

$$intracellular\ IC_{50} = unbound\ IC_{50,cell} * Kp_{uu,cell,hom} \quad (15)$$

2. Using Kp_{uu} from the saturation method (i.e., $Kp_{uu,cyto}$) at the same extracellular concentration as the unbound $IC_{50,cell}$ to predict the cytosolic IC_{50}, considering saturation effects:

$$cytosolic\ IC_{50} = unbound\ IC_{50,cell} * corresponding\ Kp_{uu,cyto} \quad (16)$$

The unbound extracellular concentration at which saturation of active mechanisms was half-maximal was calculated according to

$$unbound\ K_{m,app} = K_{m,app} * f_{u,med} \quad (17)$$

The accuracy of the prediction was expressed by the fold difference relative to $IC_{50,biochem}$.

Analytical Method. All samples were quantified using an LC-MS/MS system consisting of a CTC Analytics HTS PAL Autosampler (CTC Analytics AG, Switzerland) and Agilent 1290 Infinity System (Agilent Technologies Inc., Santa Clara, CA) coupled with an AB Sciex API4500 Triple Quad (Sciex, Framingham, MA) mass spectrometer. Sample volumes of 5 μl were injected into the system. Chromatography was performed on a Kinetex (Phenomenex Inc., Torrance, CA) C18 reverse-phase column (2.1 × 30 mm, 2.6 μm particle size) with a linear solvent gradient (flow rate: 1.2 ml/min; solvent A: H_2O + 0.1% acetic acid; solvent B: acetonitrile + 0.1% acetic acid; solvent gradient: 95% A to 95% B over 0.3 minutes). Analytes and internal standard *N*-(4-chlorophenyl)-2-[(4-piridinylmethyl)amino]-benzamide were detected in multiple reaction monitoring mode. Data analysis was performed with AB Sciex Analyst 1.6.1 software. A list with multiple reaction monitoring mass transitions and elution times for all compounds can be found in the Supplemental Material (Supplemental Table 3).

Results

Compound Selection. To study the concentration dependence of Kp_{uu}, a set of 12 KAT6A inhibitors were selected to examine intracellular target exposure in ZR75-1 cells. The test compounds were taken both from literature (WM-8014 and WM-1119, Supplemental Fig. 1) and from an internal program (compound 1–10) covering a large range in the cellular potency drop-off from little to strong discrepancies between biochemical and cellular IC_{50} values, i.e., from 1.3- to 260-fold (Table 3). The compounds show diverse physicochemical properties, with in silico $logD_{pH7.5}$ values between 1.9 and 4.5. Although most in-house compounds are acidic, i.e., carry a negative charge at the physiologic pH of 7.4, the two literature compounds are predominantly uncharged. None of the selected inhibitors contains a basic moiety, making them unsusceptible to lysosomal trapping (Schmitt et al., 2019). Compounds in the test set demonstrated good membrane permeability as confirmed by in-house Caco-2 studies (Supplemental Table 1).

Concentration-Dependent Cellular Drug Accumulation (Kp). Our hypothesis on the concentration dependence of Kp_{uu} implies that concentration-dependent changes should also be observed in the total cellular partition ratio (Kp). Indeed, cellular Kp values in ZR75-1 cells of all compounds changed over the total extracellular concentration range from 0.1 to 100 μM, typically starting from a plateau at low, nonsaturating concentrations (Kp_{unsat}), followed by a change of Kp as concentrations go up before reaching a second plateau at high, saturating concentrations (Kp_{sat}), as exemplarily shown for compound 1 in Fig. 2A and for all other KAT6A inhibitors (Supplemental Fig. 2). Curve fitting to eq. 3 was performed to determine both Kp_{unsat} and Kp_{sat}, which could be described accurately for all compounds tested ($R^2 > 0.90$) (see Table 1). The corresponding half-maximal saturation concentrations ($K_{m,app}$) cover a range from 6.8 ± 2.9 to 37.2 ± 2.2 μM. For all compounds in the test set, the upper concentrations of 100 μM were sufficient to reach at least 87% of the second plateau, i.e., the fully saturated Kp_{sat}. Because all our test compounds showed lower Kp_{unsat} compared with Kp_{sat}, either saturable drug efflux or saturable drug metabolism or both may occur at low concentrations. The presence of

significant metabolism is unlikely, as compound recovery was high at all concentrations tested, suggesting efflux to be the main driver of Kp_{unsat}. Kp_{sat} values differ largely between the KAT6A inhibitors ranging from 1.29 ± 0.04 (compound 10) to 34.5 ± 1.8 (compound 1) (see Table 1). Since all saturable processes contributing to total Kp are saturated at Kp_{sat} (Fig. 1; eq. 8), the unbound drug concentrations on both sides of the cell membrane will be equal at saturation, i.e., $Kp_{uu} = 1$. Therefore, Kp_{sat} can be used to calculate the fraction of unbound drug available to the cell cytosol ($f_{u,cyto}$) (see eq. 9). $f_{u,cyto}$, therefore, represents a new approach to derive cellular binding ($f_{u,cell}$). To distinguish the new from the classic $f_{u,cell}$ estimation, we call the Kp_{sat}-derived parameter $f_{u,cyto}$ and the cell homogenization-derived parameter $f_{u,cell,hom}$.

Comparison of $f_{u,cyto}$ and $f_{u,cell,hom}$. As a next step, the Kp_{sat}-derived estimate of the fraction of unbound drug in the cytosol ($f_{u,cyto}$) was compared with $f_{u,cell,hom}$, determined in cell homogenates, using the commonly used in vitro binding method (Mateus et al., 2013). As can be seen from Table 2, the dynamic range of $f_{u,cyto}$ [0.0000911 ± 0.0000006 (compound 3) to 0.43 ± 0.03 (WM-1119)] is much larger than that of $f_{u,cell,hom}$ [0.00015 ± 0.00007 (compound 1) to 0.16 ± 0.03 (WM-1119)]. The largest discrepancies were observed for lipophilic, highly bound compounds, such as compounds 1, 2, 3, and 9. The correlation between both parameters is only weak ($R^2 = 0.64$) (see Fig. 3A). The correlation with $logD_{pH7.5}$ was higher for $f_{u,cell,hom}$ ($R^2 = 0.76$) compared with $f_{u,cyto}$ ($R^2 = 0.48$) (see Fig. 3, B and C), indicating that $f_{u,cell,hom}$ to a greater degree depends on lipophilicity-driven membrane binding in tissue homogenates, whereas $f_{u,cyto}$ appears to carry additional information on cellular mechanisms that also contribute to intracellular unbound drug concentrations in the cytosol. Both $f_{u,cell}$ estimates, therefore, will yield different results when used to calculate Kp_{uu} (see Table 2).

Investigation of the Concentration Dependence of Kp_{uu}. In contrast to the common practice that uses $f_{u,cell,hom}$ and Kp at a single concentration, we have used concentration-dependent Kp measurements and an estimate of $f_{u,cyto}$ to examine the change of Kp_{uu} over the concentration range that is used in cellular IC_{50} assays. As can be seen in Fig. 2B, for compound 1, $Kp_{uu,cyto}$ changes from a lower value of 0.16 to approach unity at high concentrations, suggesting saturation of efflux and, hence, equal unbound drug concentrations in medium and cytosol. This behavior was seen for all compounds, although the unsaturated $Kp_{uu,cyto}$ values and the concentrations at which saturation sets in can largely vary between compounds (Supplemental Fig. 3 and Supplemental Table 2). It follows that the most accurate correction of the cellular IC_{50} requires the use of $Kp_{uu,cyto}$, determined at the very IC_{50} concentration. In contrast, the use of the unsaturated $Kp_{uu,cell,hom}$ value may not be appropriate, as cellular potency and transporter inhibition kinetics may markedly differ from compound to compound; see the large range in $K_{m,app}$ values in Table 1. Accurate Kp_{uu} correction is thus essential for all tested compounds, as their unbound intracellular concentrations are lower than their unbound extracellular concentrations, especially at the lower end of the relevant concentration range (Fig. 2C).

Prediction of Intracellular KAT6A Exposure Using $Kp_{uu,cell,hom}$ and $Kp_{uu,cyto}$ to Bridge Cellular and Biochemical Potencies. We then investigated the two different Kp_{uu} approaches regarding their corrective power to account for exposure-related discrepancies between biochemical and cellular potencies. Discrepancies were observed for all investigated KAT6A inhibitors in ZR75-1 cells, being 73-fold on average in the present compound set; see Fig. 4A. In line with the above evidence for drug efflux, all compounds were less potent in the cellular system compared with isolated KAT6A protein in biochemical inhibition studies (Table 3). In the following, we compare the two different Kp_{uu} approaches to predict the unbound drug concentrations at the intracellular target site for the KAT6A inhibitors tested:

1. Use of $Kp_{uu,cell,hom}$ to predict the intracellular IC_{50} (Fig. 4B). Using this previously published approach (Mateus et al., 2017), the gap between cellular and biochemical IC_{50} was reduced from 73- to 20-fold on average. However, for compounds that were highly bound in $f_{u,cell,hom}$ measurements (e.g., compound 1 and 9), the predicted intracellular IC_{50} became even lower than the biochemical IC_{50} (55- and 105-fold, respectively), thus resulting in a massive underprediction, which is implausible considering the compounds being subject to cellular efflux rather than active uptake in ZR75-1 cells.
2. Use of $Kp_{uu,cyto}$ that corresponds to the unbound $IC_{50,cell}$ to predict the cytosolic IC_{50} (Fig. 4C). Using this approach, the gap between biochemical and cellular potencies was reduced from an average 73-fold to an only 5.4-fold difference, leading to superior predictions compared with $Kp_{uu,cell,hom}$; see Fig. 4. Looking at all compounds in detail, we discriminated between two cases, as exemplarily shown in Fig. 5. Either the unbound cellular IC_{50} is at the fully unsaturated $Kp_{uu,cyto}$ (i.e., compound 8, Fig. 5A) or at a concentration that corresponds to a partially saturated $Kp_{uu,cyto}$ (i.e., compound 2, Fig. 5B). For 5 out of 12 compounds tested (compounds 1–5), the partially saturated rather than the fully unsaturated $Kp_{uu,cyto}$ was used for the prediction of intracellular target exposure, as saturation occurred at the unbound $IC_{50,cell}$ concentration (unbound $IC_{50,cell}$ ~ unbound $K_{m,app}$, see Supplemental Fig. 3 and Supplemental Table 2). For three of these five compounds, we saw further 2- to 3-fold improvement but no change for the other two compounds (<1.5-fold).

Discussion

The unbound partition coefficient Kp_{uu} is an emerging parameter that enables the prediction of target engagement of intracellular drug targets (Guo et al., 2018). It provides a quantitative link between biochemical and cellular potencies as recently described by Mateus et al. (2017). Surprisingly, however, Kp_{uu} is commonly used as a constant value despite the saturability of the underlying mechanisms (Fig. 1). In this study, we explore the concentration dependence of Kp_{uu} and provide a concept for drug discovery programs in which a cellular potency drop-off is observed and in which accurate predictions of intracellular drug concentrations are necessary to discriminate between target exposure and target pharmacology-related reasons (Hann and Simpson, 2014).

Concentration Dependence of Cellular Drug Disposition. For all test compounds showing a cellular potency drop-off (Fig. 4A), characteristic concentration-dependent changes in Kp_{uu} were observed (Supplemental Fig. 3). The data indicate the involvement of a saturable efflux mechanism (Table 2), resulting in overall reduced intracellular unbound drug levels in ZR75-1 cells compared with the extracellular space (Fig. 2C), suggesting that the observed cellular potency drop-off is caused by reduced intracellular target exposure and may hence be quantitatively corrected by Kp_{uu}. Since the concentration at which efflux saturation occurs largely differs between compounds (Supplemental Table 2), Kp_{uu} determined at the same extracellular concentration as the cellular IC_{50} should provide the best link between biochemical and cellular potency; see Fig. 5. Whereas for most compounds in this study, Kp_{uu} of the unsaturated state was sufficient, two compounds with relatively low cellular potency (compounds 2 and 3) showed significant efflux saturation at the cellular IC_{50}, resulting in a 5- and 22-fold difference between the relevant, partially saturated Kp_{uu} compared with the fully unsaturated Kp_{uu}. In these two cases, the partially saturated Kp_{uu} provided a better link between biochemical and cellular potency. However, since lead optimization compounds are generally optimized for high in vitro potency, it is unlikely that saturation of cellular efflux becomes relevant for highly potent

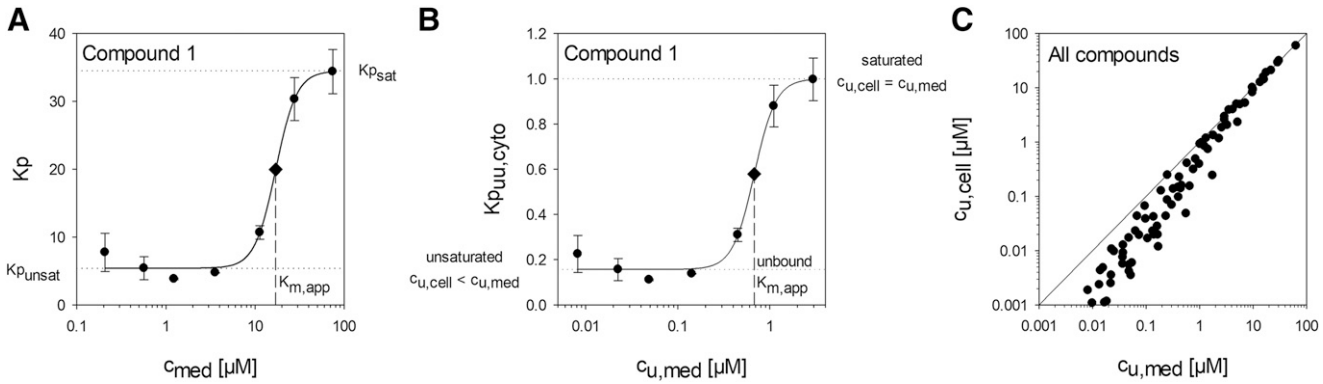

Fig. 2. Concentration-dependent cellular accumulation of KAT6A inhibitors in ZR75-1 breast cancer cells. (A) Concentration-dependent changes in total cellular accumulation ratio (Kp) of compound 1 in ZR75-1 cells allows discrimination between an unsaturated (Kp_{unsat}) and fully saturated state (Kp_{sat}). Curve fitting of eq. 3 can quantitatively describe both states and the concentration at which saturation is half-maximal ($K_{m,app}$). (B) According to our hypothesis, the cellular binding parameter $f_{u,cyto}$ can be derived from Kp_{sat} (eq. 9) and applied to subsequently determine concentration dependence of $Kp_{uu,cyto}$ (eq. 10). (C) Demonstrates the concentration-dependent relationship of unbound drug concentrations between the intracellular and extracellular space for all KAT6A inhibitors in ZR75-1 cells (measurements of all 12 compounds at seven concentration points plotted). Generally, intracellular unbound drug concentrations were reduced compared with the medium, indicating involvement of a saturable active efflux mechanism. Therefore, the unbound drug concentration asymmetry becomes less pronounced with increasing drug concentrations in the medium. Data points are expressed as means ± S.D. of triplicate measurements. c_{med} and $c_{u,med}$ represent the total and unbound concentration in the medium, respectively, and $c_{u,cell}$ the unbound concentration in the cell, i.e. in the cytosol.

compounds. Thus, the unsaturated Kp_{uu} is likely to suffice for most compounds, whereas determination of Kp_{uu} over large concentration ranges may only be necessary for low-potency compounds.

Method Simplification Approach and Rationale for Drug Discovery. Our newly introduced method to determine Kp_{uu} is generally suitable for the prediction of unbound drug concentrations in the cytosolic compartment for compounds showing a cellular potency drop-off. The simplified determination of Kp_{uu} allows for the rapid discrimination between target exposure and pharmacology-related causes. The abbreviated approach requires Kp measurements at only two concentration points and can be performed in the same assay preparation: First, the cellular Kp measured in the saturated state provides an estimate of $f_{u,cyto}$. In our study, we demonstrated that the extracellular concentration of 100 μM was sufficient to achieve close to full saturation of active cellular efflux mechanisms (Table 1). Secondly, the cellular Kp determined at a low concentration of 0.1 μM accounts for all unsaturated cellular mechanisms contributing to cellular accumulation. From Kp measurements in the saturated and unsaturated state, $Kp_{uu,cyto}$ can be calculated (eq. 11) and applied to estimate unbound intracellular target exposure. For low-potency compounds, additional Kp measurements at the same concentration as the cellular IC_{50} can provide a more accurate prediction of intracellular target exposure because saturation effects are accounted for. If a significant potency disconnect remains, it likely is not caused by differences in target exposure in the cellular assay but may rather relate to the biology of the target in the whole cell, e.g., complex pathway networks or feedback mechanisms. This novel approach to determine Kp_{uu} directly in the same cellular test system that is also used to generate cellular IC_{50} values, i.e., using the most relevant assay system, provides a very attractive alternative to the previously published binding method, in which $f_{u,cell}$ is determined in a separate assay, i.e., cell homogenization followed by equilibrium dialysis, thereby introducing additional experimental shortcomings. It has to be kept in mind that the validity of our approach is based on the assumption that saturation of active transport is achieved, that compounds remain soluble in the incubation medium throughout the concentration range used, and that no extensive drug metabolism occurs

TABLE 1

Determination of total cellular accumulation ratio for KAT6A inhibitors in the unsaturated (Kp_{unsat}) and fully saturated (Kp_{sat}) state in plated ZR75-1 cells

Parameters were obtained by curve fitting of eq. 3 to concentration-dependent Kp measurements ranging from 0.1 to 100 μM total extracellular concentration. Data are expressed as means ± S.E.

Compound	Kp_{unsat}	Kp_{sat}	$K_{m,app}$ (μM)	R^2	% Saturation [a]	% Recovery [b]
WM-8014	2.17 ± 0.09	31.5 ± 0.7	35.2 ± 1.3	0.99	87	102–94
WM-1119	1.08 ± 0.07	1.60 ± 0.09	6.8 ± 2.9	0.90	93	88–92
Compound 1	5.4 ± 0.9	34.5 ± 1.8	17.1 ± 1.9	0.99	100	87–82
Compound 2	2.5 ± 0.3	31.2 ± 1.4	37.2 ± 2.2	0.99	89	115–97
Compound 3	1.45 ± 0.09	32.9 ± 0.2	24.9 ± 0.3	0.99	97	104–91
Compound 4	1.3 ± 0.3	4.8 ± 1.0	18.0 ± 9.8	0.94	95	114–85
Compound 5	2.1 ± 0.2	10.9 ± 0.3	10.7 ± 0.7	0.99	99	102–102
Compound 6	1.5 ± 0.2	4.0 ± 0.5	8.8 ± 4.6	0.95	101	79–85
Compound 7	0.56 ± 0.06	1.70 ± 0.09	9.49 ± 0.12	0.97	92	97–106
Compound 8	0.95 ± 0.03	8.90 ± 0.05	13.0 ± 0.2	0.99	100	97–96
Compound 9	1.2 ± 0.3	5.3 ± 0.5	7.8 ± 2.0	0.97	103	97–76
Compound 10	0.49 ± 0.02	1.29 ± 0.04	11.2 ± 1.2	0.99	99	92–78

[a]Percent saturation relates to highest concentration tested, i.e., 100 μM (total). Values were calculated according to eq. 4.

[b]Compound recovery from cell and medium after the experiment (t = 45 min) related to t = 0 min, from lowest and highest initial concentration used (0.1–100 μM). Values were calculated according to eq. 2.

TABLE 2

Cellular binding and Kp_{uu} values obtained using two independent methods

$f_{u,cyto}$ was derived from Kp_{sat} (saturation method), whereas $f_{u,cell,hom}$ was measured in ZR75-1 homogenate using rapid equilibrium dialysis (binding method). Physicochemical data ($logD_{pH7.5}$) were calculated by ADMET Predictor. Data are expressed as means ± S.E.

Compound	$logD_{pH7.5}$	$f_{u,med}$	Saturation Method		Binding Method	
			$f_{u,cyto}$	$Kp_{uu,cyto}$[a]	$f_{u,cell,hom}$	$Kp_{uu,cell,hom}$[a]
WM-8014	2.9	0.180 ± 0.006	0.0057 ± 0.0001	0.069 ± 0.007	0.025 ± 0.003	0.30 ± 0.06
WM-1119	1.9	0.69 ± 0.03	0.43 ± 0.03	0.68 ± 0.11	0.16 ± 0.03	0.26 ± 0.08
Compound 1	4.5	0.040 ± 0.005	0.00115 ± 0.00006	0.16 ± 0.05	0.00015 ± 0.00007	0.02 ± 0.01
Compound 2	2.8	0.0114 ± 0.0006	0.00036 ± 0.00002	0.08 ± 0.02	0.0064 ± 0.0004	1.4 ± 0.3
Compound 3	3.1	0.00299 ± 0.00008	0.0000911 ± 0.0000006	0.044 ± 0.004	0.0005 ± 0.0002	0.25 ± 0.12
Compound 4	2.3	0.26 ± 0.01	0.05 ± 0.01	0.26 ± 0.12	0.051 ± 0.006	0.25 ± 0.10
Compound 5	2.7	0.16 ± 0.01	0.0145 ± 0.0004	0.19 ± 0.03	0.0110 ± 0.0009	0.14 ± 0.03
Compound 6	2.4	0.37 ± 0.03	0.09 ± 0.01	0.38 ± 0.13	0.053 ± 0.007	0.22 ± 0.08
Compound 7	1.9	0.130 ± 0.003	0.077 ± 0.004	0.33 ± 0.06	0.076 ± 0.004	0.32 ± 0.06
Compound 8	2.6	0.05 ± 0.01	0.00592 ± 0.00004	0.11 ± 0.02	0.0017 ± 0.0004	0.03 ± 0.01
Compound 9	2.9	0.130 ± 0.005	0.025 ± 0.002	0.22 ± 0.08	0.005 ± 0.002	0.05 ± 0.03
Compound 10	2.1	0.375 ± 0.003	0.29 ± 0.01	0.38 ± 0.03	0.03 ± 0.01	0.05 ± 0.02

[a]For the calculation of Kp_{uu} values, the Kp in the fully unsaturated state (Kp_{unsat}) was used for both methods (eqs. 10 and 14).

in the course of the assay. This can be ensured by including a mass balance analysis in the study protocol.

Method Differences ($f_{u,cyto}$ vs. $f_{u,cell,hom}$), Assumptions, and Limitations. Method-dependent differences in the determination of $f_{u,cyto}$ and $f_{u,cell,hom}$ were observed, suggesting that the two approaches differently reflect the processes that contribute to the unbound intracellular fraction. A recent study demonstrated that $f_{u,cell,hom}$ largely depends on lipophilicity-driven membrane partitioning, as binding to phospholipid-coated beads was superior to logD (Treyer et al., 2018; Treyer et al., 2019). The physiologic representation of cellular binding thus seems to be an important aspect for the accurate estimation of $f_{u,cell}$. The proposed $f_{u,cyto}$ assay most closely reflects the physiologic conditions since the cells remain fully intact and are not subjected to cellular disruption, unlike the cell homogenization assay, which disintegrates cells and their subcellular compartments to membrane fractions. The possible generation of artificial binding sites in tissue homogenates may impact binding measurements and could be one explanation for the low $f_{u,cell,hom}$ values observed in previously reported studies (Riede et al., 2017; Guo et al., 2018). Furthermore, overestimation of binding can also occur because of extensive homogenate dilution and inaccurate scaling (eq. 13) of the dilution factor D (Riccardi et al., 2018). As eq. 13 originates from plasma protein binding and assumes a single binding site per binding partner (Banker et al., 2003), its applicability to tissue homogenates may be limited. Large numbers of cells are needed for homogenates to reduce dilution-related inaccuracies, requiring timely and cost-intensive cultivation. The method is particularly error-prone for highly bound compounds, common in early drug discovery, often suffering from poor compound recovery from the dialysis receiver chamber (Schuhmacher et al., 2004). In contrast to these shortcomings, our approach to determine $f_{u,cyto}$ provides an estimate of all processes that contribute to cellular binding in the intact cellular system at physiologic conditions using a single assay format that 1) relates to the unbound drug concentration in the cytosol, 2) directly relates to the cellular IC_{50} assay, and 3) does not require additional cell homogenization and equilibrium dialysis assays. Furthermore, as high Kp_{sat} values are indicative of low $f_{u,cyto}$, this approach is suitable to overcome frequently observed detection limits of LC-MS/MS–based compound quantification for highly bound compounds in the equilibrium dialysis (e.g., compound 3, $f_{u,cyto}$ = 0.0000911). These may be reasons why large differences between $f_{u,cell,hom}$ and $f_{u,cyto}$ were

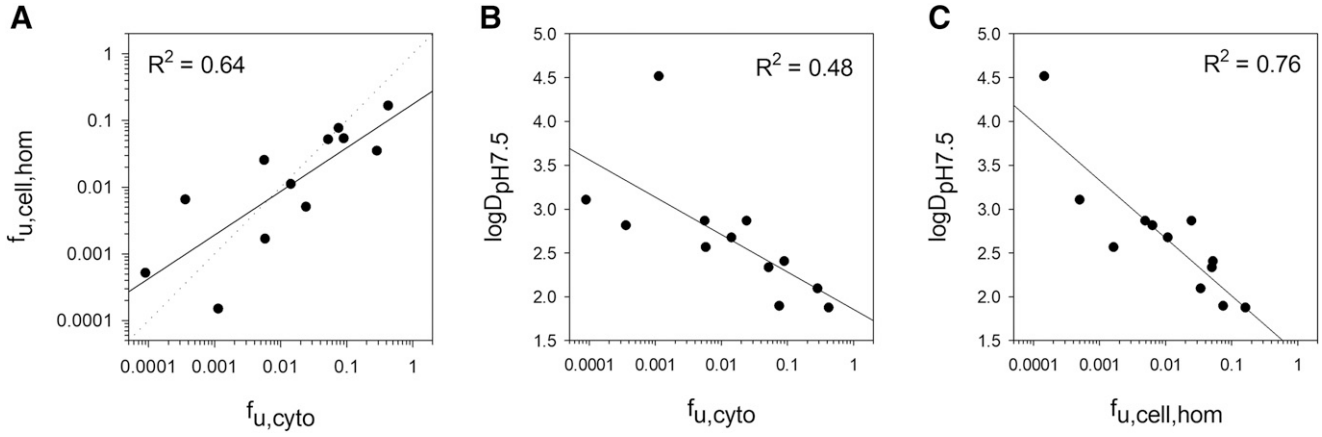

Fig. 3. Comparison of $f_{u,cell}$ estimates obtained with the two different methods. $f_{u,cell,hom}$ is determined in tissue homogenates using equilibrium dialysis, whereas $f_{u,cyto}$ was derived from measurements of concentration-dependent cellular accumulation. (A) A poor correlation between both parameters was observed, indicating that they carry different information regarding cellular binding. Better correlation with in silico predicted $logD_{pH7.5}$ values of $f_{u,cell,hom}$ (C) compared with $f_{u,cyto}$ (B) suggests that binding measurements in cell homogenates are mostly representative of lipophilicity-driven membrane partitioning, whereas the nondestructive saturation method–derived parameter $f_{u,cyto}$ could include additional information with regard to the mechanism involved in cellular disposition. Subsequently, different Kp_{uu} values are generated depending on the method that is used for the estimation of $f_{u,cell}$.

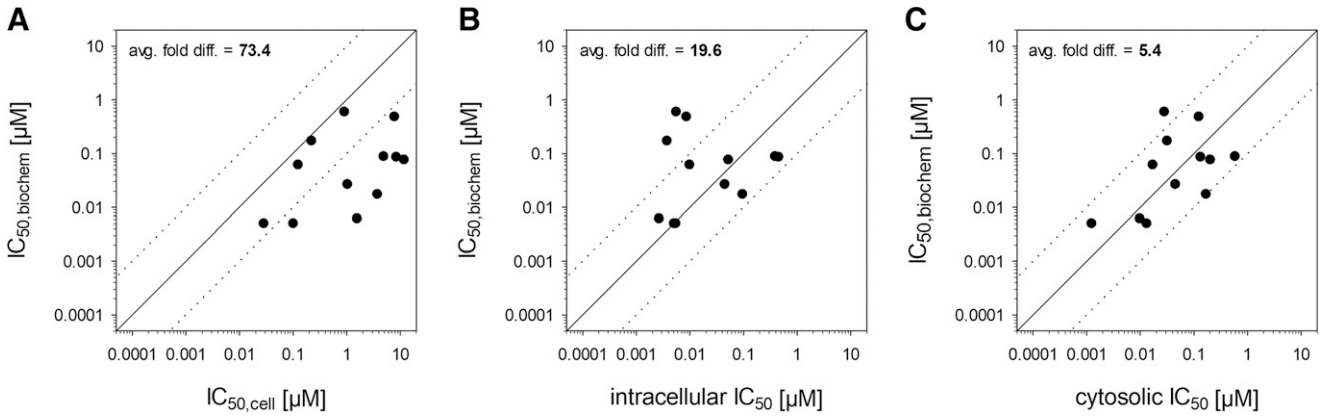

Fig. 4. (A) Disconnect between in vitro cellular and biochemical potencies of KAT6A inhibitors. Reduced potency against ZR75-1 cells compared with isolated KAT6A demonstrates the "cellular drop-off." (B) Prediction of intracellular target exposure using $Kp_{uu,cell,hom}$ from the binding method was able to reduce the disconnect. (C) Further improvement was observed when using the saturation-derived parameter $Kp_{uu,cyto}$ for the prediction of cytosolic target exposure under consideration of efflux saturability. Dotted lines represent a 10-fold difference relative to the biochemical potency.

observed for most compounds in this study (Fig. 3A), resulting in different Kp_{uu} values. We compared both approaches regarding their power to predict intracellular KAT6A exposure for compounds with deviant biochemical and cellular IC_{50} values. Whereas $Kp_{uu,cell,hom}$ determined with the binding method and not considering saturability was able to reduce the observed potency disconnect between biochemical and cellular IC_{50} from 73- to 20-fold on average (Fig. 4, A and B), both highly bound and low-potency compounds were apparently predicted to be more potent in ZR75-1 cells compared with isolated KAT6A (i.e., compounds 1, 9, and 10: 45-, 55-, and 105-fold underprediction, respectively; Table 3). This is implausible because these compounds are effluxed from ZR75-1 cells rather than being pumped in. Interpretations using $Kp_{uu,cell,hom}$ thus erroneously led to the suggestion that the cellular pharmacology of the target might have been the main source of the discrepancies to the biochemical potency. In contrast, $Kp_{uu,cyto}$ predicts an intracellular target exposure that reduces the potency disconnect down to only 5.4-fold on average (Fig. 4, A and C). The observed potency disconnect can thus largely be reconciled by accounting for intracellular target exposure, and speculations on complex cellular target pharmacology are not required for the observed "cell drop-off" in ZR75-1. This conclusion is also fully consistent with the observed efflux of the compounds. Our method therefore allows a more reliable quantitative link between biochemical and cellular IC_{50} assay and thus carries more power to guide lead optimization.

Implications of Concentration-Dependent Kp_{uu} for In Vivo Pharmacokinetics and Prediction of Unbound Tissue Concentrations. In this study, we show that Kp_{uu} is not constant over large concentration ranges, as it depends on the net saturation of the involved mechanisms. This property of Kp_{uu} should be taken into account when looking at in vivo pharmacokinetic profiles often showing large changes of plasma concentrations over time and hence different levels of saturation of, e.g., hepatic transporters (Sato et al., 2018), contributing to nonlinear pharmacokinetics. Therefore, we suggest that in vitro $Kp_{uu,cyto}$ should be determined in the range of the relevant in vivo unbound plasma concentrations to reflect potential saturation effects and thereby improve in vitro–to–in vivo extrapolation, drug-drug interaction, and hepatic clearance predictions as well as predictions of in vivo unbound intracellular target concentrations.

Conclusions

In this study, we have investigated the concentration dependence of the unbound partition coefficient Kp_{uu} in vitro. Our study gave rise to a novel approach, i.e., the determination of $Kp_{uu,cyto}$, which 1) improves

TABLE 3

Prediction of intracellular KAT6A target exposure using two independent methods and comparison with biochemical potency measurements

Compound	$IC_{50,biochem}$ (μM)	$IC_{50,cell}$ (μM)	Fold Difference Relative to $IC_{50,biochem}$	Saturation Method[a]		Binding Method[b]	
				Cytosolic IC_{50} (μM)	Fold Difference Relative to $IC_{50,biochem}$	Intracellular IC_{50} (μM)	Fold Difference Relative to $IC_{50,biochem}$
WM-8014	0.005	0.10	20	0.001	4.0	0.006	1.1
WM-1119	0.005	0.03	5.7	0.013	2.7	0.005	1.0
Compound 1	0.48	7.8	16	0.12	3.8	0.009	55
Compound 2	0.085	8.52	100	0.13	1.6	0.46	5.4
Compound 3	0.075	12	158	0.20	2.7	0.053	1.4
Compound 4	0.088	4.9	57	0.59	6.8	0.39	4.5
Compound 5	0.017	3.8	220	0.17	9.9	0.097	5.6
Compound 6	0.061	0.12	2.1	0.017	3.5	0.010	6.1
Compound 7	0.026	1.0	40	0.046	1.7	0.045	1.7
Compound 8	0.006	1.6	260	0.010	1.6	0.003	2.3
Compound 9	0.59	0.92	1.5	0.029	21	0.006	105
Compound 10	0.17	0.22	1.3	0.032	5.3	0.004	45

[a]For the prediction of cytosolic IC_{50}, the $Kp_{uu,cyto}$ at the unbound $IC_{50,cell}$ was used (eq. 16).
[b]For the prediction of intracellular IC_{50}, the $Kp_{uu,cell,hom}$ in the unsaturated state was used (eq. 15).

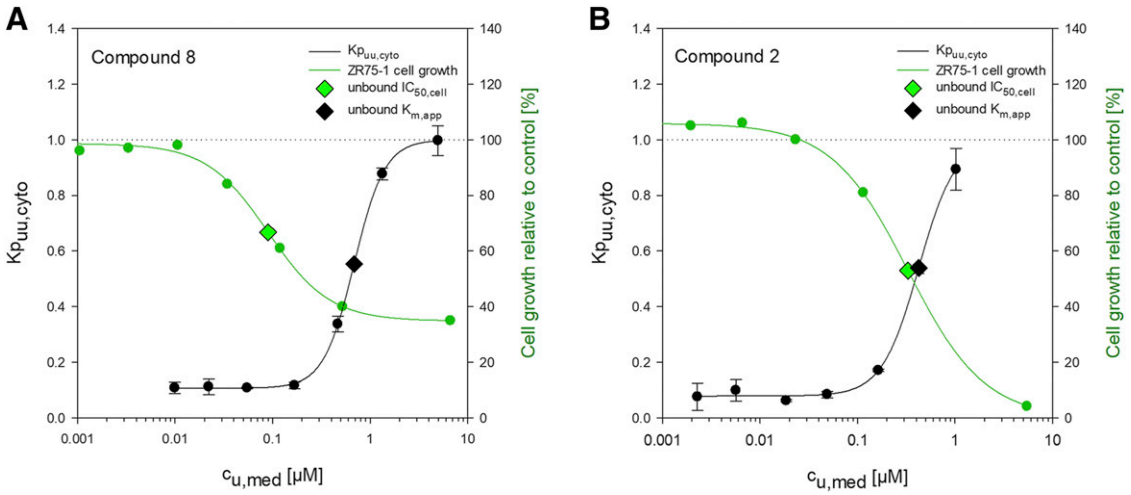

Fig. 5. Concentration-dependent $Kp_{uu,cyto}$ and unbound cellular in vitro potency of selected KAT6A inhibitors compound 8 (A) and compound 2 (B). For compound 8, the unbound cellular IC50 was determined at a concentration in which no efflux saturation occurred. For the prediction of cytosolic target exposure, $Kp_{uu,cyto}$ in the unsaturated state was used. At the unbound $IC_{50,cell}$ of compound 2, saturation of efflux was relevant, and a partially saturated $Kp_{uu,cyto}$ was used for the prediction of cytosolic target exposure. Data points are expressed as means ± S.D. of triplicate measurements. $c_{u,med}$ represents the unbound concentration in the medium.

the prediction of unbound intracellular target exposure and 2) overcomes shortcomings of the commonly used binding method. We highlight the importance of saturation effects that occur in vitro as well as in vivo that previously have not been accounted for in the determination of Kp_{uu}, making the prediction of unbound cytosolic drug concentrations more accurate. It may be of interest to see how this assay will perform for basic lipophilic drugs that undergo extensive lysosomal trapping, which is not reflected in $f_{u,cell}$ values obtained by the homogenization method but is potentially covered by the proposed method.

Acknowledgments

We would like to thank Frank Igogeit for his support in LC-MS/MS compound quantification, Uta Reckling and Ulla Mönning for generation of the Caco-2 data, as well as Stephan Menz for assistance regarding mathematical questions and Stefan Gradl for very helpful discussions. We are also grateful to Lisa Schälicke, Ulrike Grothe, Stefanie, Marion Sentz-Szymanski, Jana Hannig, Mandy Busch, and Nicole Dittmar for their laboratory work.

Authorship Contributions

Participated in research design: Trünkle, Lechner, Süssmuth. Reichel.

Conducted experiments: Trünkle, Korr, Barak, Fernández-Montalván.

Contributed new reagents or analytic tools: Korr, Bouché.

Performed data analysis: Trünkle, Lechner, Korr, Barak, Fernández-Montalván, Reichel.

Wrote or contributed to the writing of the manuscript: Trünkle, Lechner, Süssmuth, Reichel.

References

Alberts B (2008) *Molecular Biology of the Cell*, Garland Science, New York.

Baell JB, Leaver DJ, Hermans SJ, Kelly GL, Brennan MS, Downer NL, Nguyen N, Wichmann J, McRae HM, Yang Y, et al. (2018) Inhibitors of histone acetyltransferases KAT6A/B induce senescence and arrest tumour growth. *Nature* **560**:253–257.

Banker MJ, Clark TH, and Williams JA (2003) Development and validation of a 96-well equilibrium dialysis apparatus for measuring plasma protein binding. *J Pharm Sci* **92**:967–974.

Dreveny I, Deeves SE, Fulton J, Yue B, Messmer M, Bhattacharya A, Collins HM, and Heery DM (2014) The double PHD finger domain of MOZ/MYST3 induces α-helical structure of the histone H3 tail to facilitate acetylation and methylation sampling and modification. *Nucleic Acids Res* **42**:822–835.

Faneyte IF, Kristel PM, and van de Vijver MJ (2001) Determining MDR1/P-glycoprotein expression in breast cancer. *Int J Cancer* **93**:114–122.

Guo Y, Chu X, Parrott NJ, Brouwer KLR, Hsu V, Nagar S, Matsson P, Sharma P, Snoeys J, Sugiyama Y, et al.; International Transporter Consortium (2018) Advancing predictions of tissue and intracellular drug concentrations using in vitro, imaging and physiologically based pharmacokinetic modeling approaches. *Clin Pharmacol Ther* **104**:865–889.

Hann MM and Simpson GL (2014) Intracellular drug concentration and disposition--the missing link? *Methods* **68**:283–285.

Lemos C, Kathmann I, Giovannetti E, Beliën JA, Scheffer GL, Calhau C, Jansen G, and Peters GJ (2009) Cellular folate status modulates the expression of BCRP and MRP multidrug transporters in cancer cell lines from different origins. *Mol Cancer Ther* **8**:655–664.

Li Q, Zhou T, Wu F, Li N, Wang R, Zhao Q, Ma YM, Zhang JQ, and Ma BL (2018) Subcellular drug distribution: mechanisms and roles in drug efficacy, toxicity, resistance, and targeted delivery. *Drug Metab Rev* **50**:430–447.

Mateus A, Gordon LJ, Wayne GJ, Almqvist H, Axelsson H, Seashore-Ludlow B, Treyer A, Matsson P, Lundbäck T, West A, et al. (2017) Prediction of intracellular exposure bridges the gap between target- and cell-based drug discovery. *Proc Natl Acad Sci USA* **114**: E6231–E6239.

Mateus A, Matsson P, and Artursson P (2013) Rapid measurement of intracellular unbound drug concentrations. *Mol Pharm* **10**:2467–2478.

Montanari F, Kuhnke L, Ter Laak A, and Clevert DA (2019) Modeling physico-chemical ADMET endpoints with multitask graph convolutional networks. *Molecules* **25**:E44.

Naim B, Brumfeld V, Kapon R, Kiss V, Nevo R, and Reich Z (2007) Passive and facilitated transport in nuclear pore complexes is largely uncoupled. *J Biol Chem* **282**:3881–3888.

Nguyen D, Lemos C, Wortmann L, Eis K, Holton SJ, Boemer U, Moosmayer D, Eberspaecher U, Weiske J, Lechner C, et al. (2019) Discovery and characterization of the potent and highly selective (Piperidin-4-yl)pyrido[3,2- d]pyrimidine based in vitro probe BAY-885 for the kinase ERK5. *J Med Chem* **62**:928–940.

Oba T, Izumi H, and Ito KI (2016) ABCB1 and ABCC11 confer resistance to eribulin in breast cancer cell lines. *Oncotarget* **7**:70011–70027.

Rajendran L, Knölker HJ, and Simons K (2010) Subcellular targeting strategies for drug design and delivery. *Nat Rev Drug Discov* **9**:29–42.

Riccardi K, Ryu S, Lin J, Yates P, Tess D, Li R, Singh D, Holder BR, Kapinos B, Chang G, et al. (2018) Comparison of species and cell-type differences in fraction unbound of liver tissues, hepatocytes, and cell lines. *Drug Metab Dispos* **46**:415–421.

Riede J, Camenisch G, Huwyler J, and Poller B (2017) Current In Vitro methods to determine hepatic Kp_{uu}: a comparison of their usefulness and limitations. *J Pharm Sci* **106**: 2805–2814.

Sato M, Toshimoto K, Tomaru A, Yoshikado T, Tanaka Y, Hisaka A, Lee W, and Sugiyama Y (2018) Physiologically based pharmacokinetic modeling of bosentan identifies the saturable hepatic uptake as a major contributor to its nonlinear pharmacokinetics. *Drug Metab Dispos* **46**: 740–748.

Schmitt MV, Lienau P, Fricker G, and Reichel A (2019) Quantitation of lysosomal trapping of basic lipophilic compounds using in vitro assays and in silico predictions based on the determination of the full pH profile of the endo-/lysosomal system in rat hepatocytes. *Drug Metab Dispos* **47**:49–57.

Schuhmacher J, Kohlsdorfer C, Bühner K, Brandenburger T, and Kruk R (2004) High-throughput determination of the free fraction of drugs strongly bound to plasma proteins. *J Pharm Sci* **93**: 816–830.

Sheikh BN, Phipson B, El-Saafin F, Vanyai HK, Downer NL, Bird MJ, Kueh AJ, May RE, Smyth GK, Voss AK, et al. (2015) MOZ (MYST3, KAT6A) inhibits senescence via the INK4A-ARF pathway. *Oncogene* **34**:5807–5820.

Sugano K, Kansy M, Artursson P, Avdeef A, Bendels S, Di L, Ecker GF, Faller B, Fischer H, Gerebtzoff G, et al. (2010) Coexistence of passive and carrier-mediated processes in drug transport. *Nat Rev Drug Discov* **9**:597–614.

Timney BL, Raveh B, Mironska R, Trivedi JM, Kim SJ, Russel D, Wente SR, Sali A, and Rout MP (2016) Simple rules for passive diffusion through the nuclear pore complex. *J Cell Biol* **215**: 57–76.

Treyer A, Mateus A, Wiśniewski JR, Boriss H, Matsson P, and Artursson P (2018) Intracellular drug bioavailability: effect of neutral lipids and phospholipids. *Mol Pharm* **15**: 2224–2233.

Treyer A, Walday S, Boriss H, Matsson P, and Artursson P (2019) A cell-free approach based on phospholipid characterization for determination of the cell specific unbound drug fraction ($f_{u,cell}$). *Pharm Res* **36**:178.

Varma MV, Steyn SJ, Allerton C, and El-Kattan AF (2015) Predicting clearance mechanism in drug discovery: extended clearance classification system (ECCS). *Pharm Res* **32**:3785–3802.

Yoshikado T, Toshimoto K, Nakada T, Ikejiri K, Kusuhara H, Maeda K, and Sugiyama Y (2017) Comparison of methods for estimating unbound intracellular-to-medium concentration ratios in rat and human hepatocytes using statins. *Drug Metab Dispos* **45**:779–789.

Yu L, Liang Y, Cao X, Wang X, Gao H, Lin SY, Schiff R, Wang XS, and Li K (2017) Identification of MYST3 as a novel epigenetic activator of ERα frequently amplified in breast cancer. *Oncogene* **36**:2910–2918.

Zhang D, Hop CECA, Patilea-Vrana G, Gampa G, Seneviratne HK, Unadkat JD, Kenny JR, Nagapudi K, Di L, Zhou L, et al. (2019) Drug concentration asymmetry in tissues and plasma for small molecule-related therapeutic modalities. *Drug Metab Dispos* **47**:1122–1135.

Zheng N, Tsai HN, Zhang X, and Rosania GR (2011) The subcellular distribution of small molecules: from pharmacokinetics to synthetic biology. *Mol Pharm* **8**:1619–1628.

Address correspondence to: Dr. Andreas Reichel, Bayer AG, Pharma R&D, Research Pharmacokinetics, Bldg. S109, 612, 13342 Berlin, Germany. E-mail: andreas.reichel@bayer.com

Supplemental Material to DMD/2020/090563

Concentration dependency of the unbound partition coefficient Kp_{uu} and its application to correct for exposure related discrepancies between biochemical and cellular potency of KAT6A inhibitors

Trünkle C., Lechner C., Korr D., Bouché L., Barak N., Fernández-Montalván A., Süssmuth R.D. and Reichel A.

Drug Metabolism and Disposition

A

WM-8014

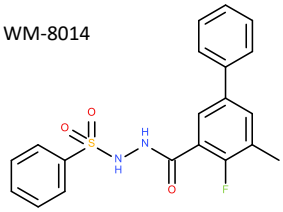

B

WM-1119

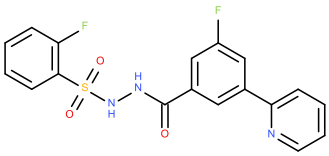

Supplemental Figure 1: Chemical structure of previously published KAT6A inhibitors WM-8014 (A) and WM-1119 (B) that were included in this study.

Concentration dependency of the unbound partition coefficient Kp_{uu} and its application to correct for exposure related discrepancies between biochemical and cellular potency of KAT6A inhibitors

Trünkle C., Lechner C., Korr D., Bouché L., Barak N., Fernández-Montalván A., Süssmuth R.D. and Reichel A.

Drug Metabolism and Disposition

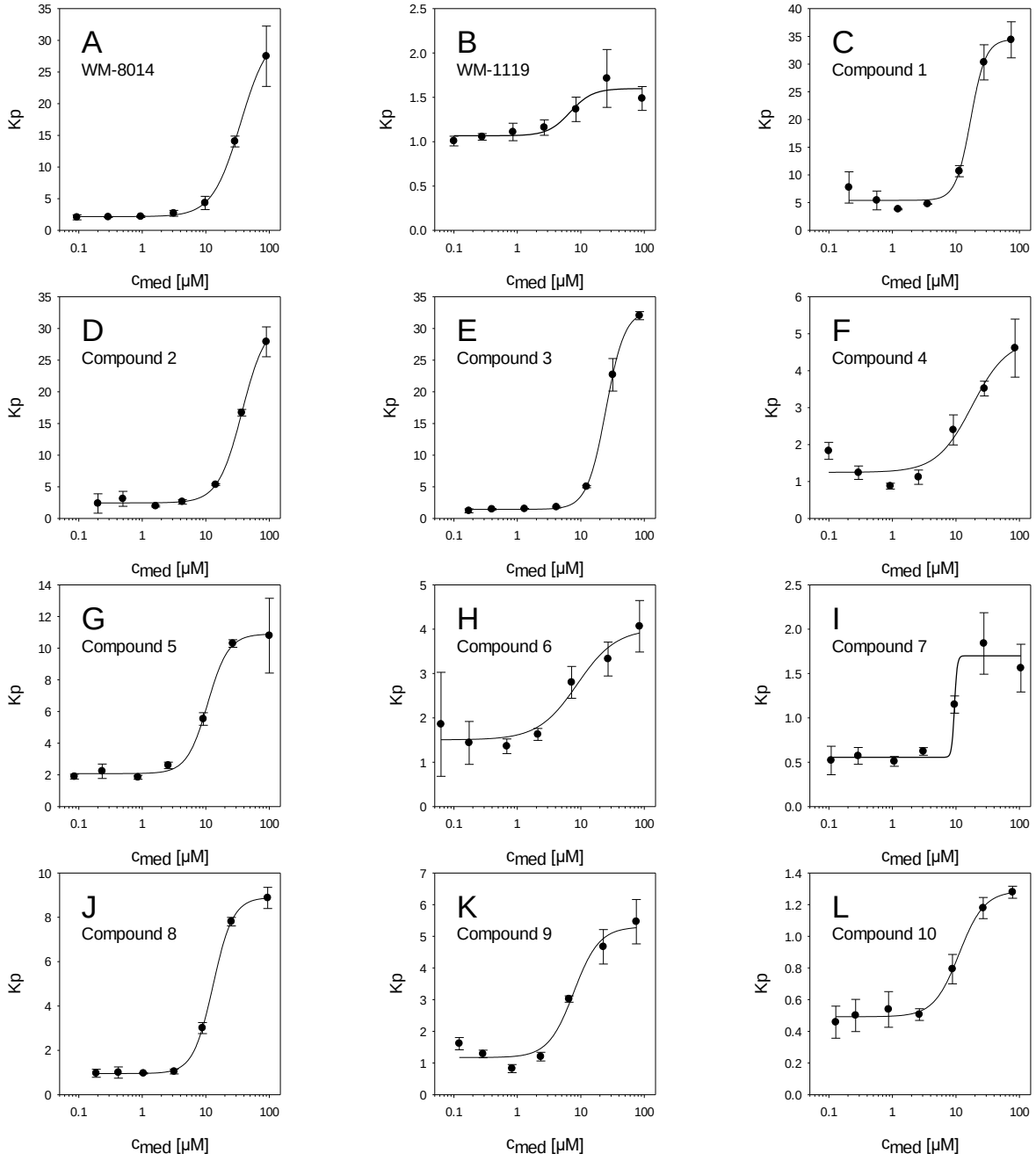

Supplemental Figure 2: Concentration dependent cellular accumulation ratio (Kp) in ZR75-1 cells for all investigated KAT6A inhibitors in this study (A-L). The line represents curve fitting of Eq. 3 to the data points to estimate Kp_{sat} and $K_{m,app}$. The accuracy of $f_{u,cyto}$ estimates depends on how reliable Kp_{sat} can be estimated.

Concentration dependency of the unbound partition coefficient Kp_{uu} and its application to correct for exposure related discrepancies between biochemical and cellular potency of KAT6A inhibitors

Trünkle C., Lechner C., Korr D., Bouché L., Barak N., Fernández-Montalván A., Süssmuth R.D. and Reichel A.

Drug Metabolism and Disposition

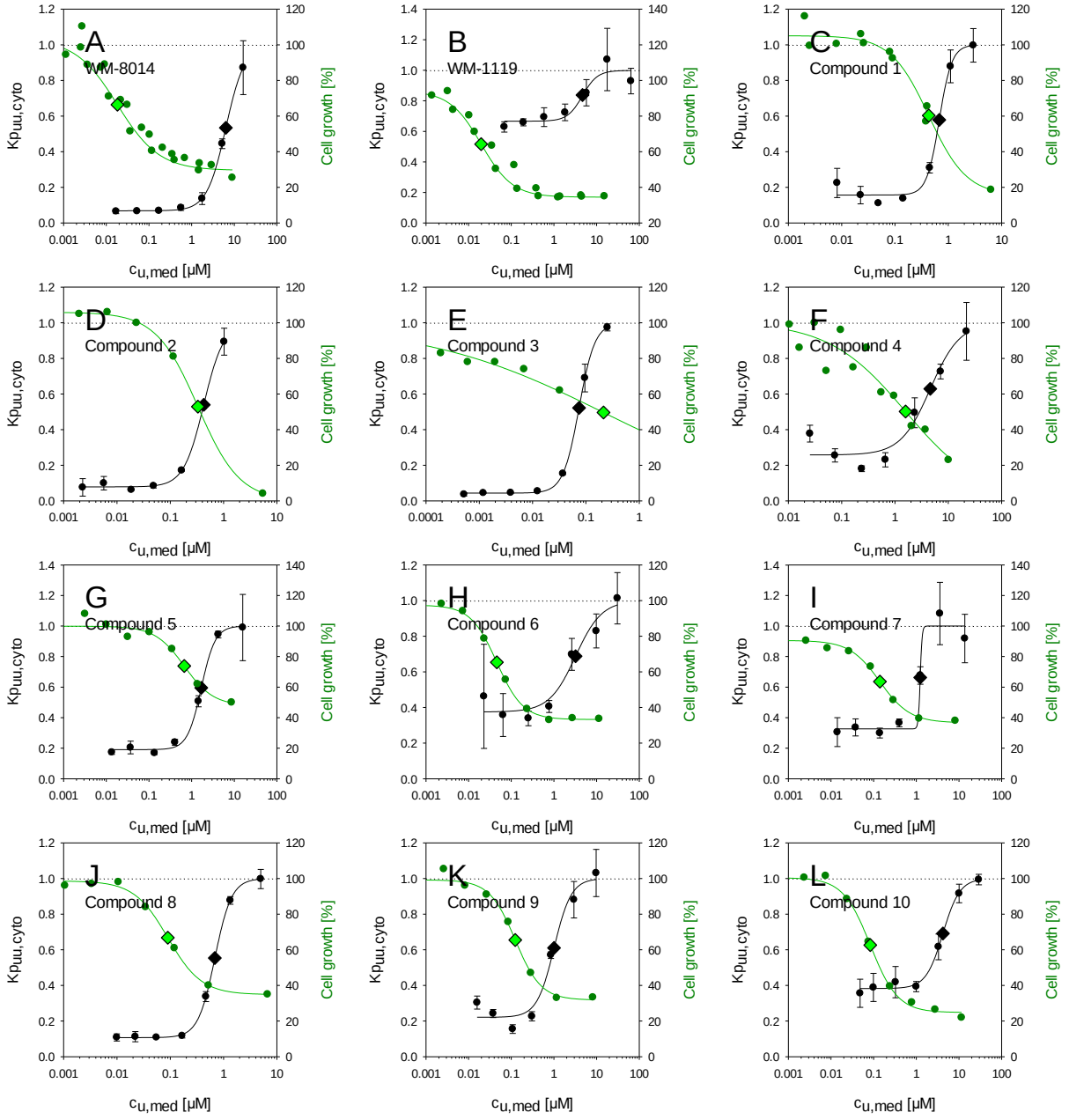

Supplemental Figure 3: Concentration dependent $Kp_{uu,cyto}$ determined with the saturation method and observed *in vitro* potency against ZR75-1 cells for all KAT6A inhibitors in this study (A-L).

Supplemental Table 1: *In silico* physicochemical compound properties of KAT6A inhibitors calculated by ADMET Predictor™ and *in vitro* Caco-2 permeability.

Compound	*In silico* prediction of physicochemical properties			Caco-2 P_{app} [nm/s] [a]
	$logD_{pH7.5}$	acidic pk_a	Predominant charge state at pH = 7.4	
WM-8014	2.9	8.8	neutral	260
WM-1119	1.9	7.7	neutral	197
Compound 1	4.5	7.6	neutral	n.d.
Compound 2	2.8	3.6	negative	55
Compound 3	3.1	3.6	negative	96
Compound 4	2.3	4.1	negative	67
Compound 5	2.7	3.8	negative	95
Compound 6	2.4	4.3	negative	146
Compound 7	1.9	4.1	negative	53
Compound 8	2.6	4.1	negative	238
Compound 9	2.9	3.7	negative	223
Compound 10	2.1	3.8	negative	n.d.

n.d.: not determined

[a] *Caco-2 permeability data was determined during routine compound characterization*

Supplemental Table 2: Relevance of cellular saturation effects that occur at the unbound $IC_{50,cell}$ for the prediction of intracellular KAT6A exposure.

Compound	Unbound $IC_{50,cell}$ [µM]	Unbound $K_{m,app}$ [µM]	Unbound $IC_{50,cell}$ ~ Unbound $K_{m,app}$	Difference between unsaturated and corresponding $Kp_{uu,cyto}$	Prediction improvement using corresponding $Kp_{uu,cyto}$
WM-8014	0.018	6.3 ± 0.4	no	-	-
WM-1119	0.019	4.7 ± 2.2	no	-	-
Compound 1	0.43	0.68 ± 0.16	yes	1.8-fold	1.9-fold
Compound 2	0.33	0.42 ± 0.05	yes	5.2-fold	2.1-fold
Compound 3	0.22	0.074 ± 0.003	yes	22-fold	3.0-fold
Compound 4	1.6	4.6 ± 2.8	yes	1.5-fold	-
Compound 5	0.67	1.69 ± 0.23	yes	1.3-fold	-
Compound 6	0.046	3.2 ± 1.9	no	-	-
Compound 7	0.14	1.24 ± 0.04	no	-	-
Compound 8	0.090	0.69 ± 0.14	no	-	-
Compound 9	0.12	1.0 ± 0.3	no	-	-
Compound 10	0.083	4.2 ± 0.5	no	-	-

Supplemental Table 3: Analytical method parameters for compound quantification via LC-MS/MS.

Compound	MW [g/mol]	RT [min]	Ionization Method	Q_1 [Da]	CE [eV]	Q_3 [Da]
WM-8014	384.4	0.41	ESI +	384.9	23	213.0
WM-1119	389.4	0.37	ESI +	389.9	69	172.0
Compound 1	460.5	0.45	ESI -	459.0	-34	140.8
Compound 2	510.2	0.53	ESI -	508.6	-38	225.7
Compound 3	602.7	0.54	ESI -	600.5	-38	189.8
Compound 4	437.5	0.43	ESI +	437.9	29	216.9
Compound 5	455.9	0.46	ESI +	455.9	25	163.0
Compound 6	420.5	0.44	ESI +	421.0	29	204.0
Compound 7	443.5	0.38	ESI +	426.9	33	205.0
Compound 8	435.5	0.45	ESI -	434.1	-44	145.8
Compound 9	434.5	0.44	ESI -	433.1	-40	168.8
Compound 10	410.4	0.40	ESI -	409.0	-82	143.9
Internal Standard	337.8	0.35	ESI +	337.9	25	210.9
Internal Standard	337.8	0.35	ESI -	335.9	-22	208.8

MW: Molecular Weight; RT: Retention Time; CE: Collision Energy; Q_1: Parent analyte mass; Q_2: Daughter analyte mass